RSC Pharmaceutics

ROYAL SOCIETY OF CHEMISTRY

PAPER

Published on 03 September 2026

Cite this: DOI: 10.1039/d6pm00199h

Formulation of an ultra-high concentration aqueous antibody particle suspension

Talia Zheng and Patrick S. Doyle *

Received 27th May 2026,
Accepted 25th August 2026

DOI: 10.1039/d6pm00199h

rsc.li/RSCPharma

The need for ultra-high concentration antibody formulations is growing due to the emergence of subcutaneous (SC) delivery as the preferred administration route for antibodies and other biologics. The high dosage requirements for immunotherapies and limited injection volume for the subcutaneous space necessitate increasingly concentrated antibody formulations, but typical high-concentration antibody solutions face instabilities and high viscosities. Previous work has shown that solid antibodies encapsulated in hydrogel microparticles improve the stability and injectability of antibodies, but have been limited in formulation concentration (<400 mg mL^{-1}), particle diameter size (>60 μm), and throughput. In this work, we optimize the formulation for a solvent-based dehydration and precipitation platform to achieve an ultra-high concentration (up to 480 mg mL^{-1}) solid antibody-laden hydrogel microparticle suspension. The suspension (7–32 μm diameter) meets clinical injectability standards with glide force <20 N, and the antibody displays structural and functional stability over 4 months at this ultra-high concentration. This work represents a new upper limit on antibody concentration in an aqueous formulation, ideal for enabling SC administration.

Introduction

Monoclonal antibodies and other biologics as immunotherapies have been formative in the treatment landscape for cancers, auto-immune diseases, and other chronic and acute conditions.[1] These therapies are typically administered *via* the intravenous (IV) route, but in recent years, subcutaneous (SC) delivery has been emerging as the preferred administration route for antibodies and therapeutic proteins due to its accessibility and reduced patient burden.[2,3] In SC delivery, the injection volume is limited (<2 mL), necessitating the formulation of high-concentration (>200 mg mL^{-1}) antibodies. However, typical high-concentration antibody solutions are unstable and difficult to inject, due to molecular interactions between the antibodies which lead to instabilities and high viscosities in solution.[4,5] The challenges in formulating high-concentration antibodies can significantly delay the time to clinical trials and product launches.[6] Currently, there are 45 monoclonal antibody (mAb) products for SC delivery on the market with a concentration ≥100 mg mL^{-1}. The highest concentration found among these formulations is 200 mg mL^{-1}, while most mAb therapies require doses of at least 200 mg.[7] Due to this high dosing requirement, it is desired to formulate antibodies at sufficiently high concentrations to deliver these large doses in compact volumes (~1 mL).

Solid antibodies encapsulated in hydrogel microparticles have been shown to improve the stability and injectability of highly concentrated antibodies.[8,9] Previously, an IgG antibody was formulated in aqueous suspension at >300 mg mL^{-1} using this hydrogel encapsulation method.[10] Droplets of IgG solution, with a poly(ethylene)glycol (PEG) precipitant and an alginate polymer, were concentrated *via* a solvent-based dehydration process. The concentration of PEG and IgG in the droplet induced precipitation of the antibody into an amorphous solid dispersion (ASD). Simultaneously, the alginate was ionically cross-linked, which formed an ASD-laden hydrogel particle, where the particle loading was high due to the extraction of water by the solvent. The particles were then suspended in a solution with PEG so the antibody remained solid and encapsulated by the hydrogel. The antibody is more stable in an ASD compared to a solution, and the lubricious, shear-thinning hydrogel reduces the viscosity of the particle formulation while masking antibody–antibody interactions. Previous work showed that a 300 mg mL^{-1} solid mAb formulation had an approximate two-fold reduction in viscosity at high shear rates when encapsulated in a hydrogel compared to the suspension form.[11] Notably, the final dosage form was in an aqueous medium, unlike many high-concentration antibody formulations that use non-aqueous carriers, which face clinical and regulatory challenges.[12] While this formulation was shown to be injectable and stable at 360 mg mL^{-1}, there is a need for ultra-high (>400 mg mL^{-1}) antibody formulations, which can meet the higher dosage requirements of immune-related therapies and enable at-home administration of antibody

Department of Chemical Engineering, 400 Main Street, Cambridge, MA 02139, USA. E-mail: pdoyle@mit.edu

therapies with improved convenience and ease of delivery.[5,13,14]

In this work, we present the formulation of an ultra-high concentration antibody particle suspension. We make use of the previously developed solvent-based dehydration process to produce ASD-laden hydrogel particles and optimize formulation parameters to achieve particle loadings >600 mg mL^{-1}, leading to a final formulation concentration of 450–480 mg mL^{-1}. The increase in formulation concentration results in up to 25% reduction in injection volume compared to the previous formulation. We also show the production of microparticles using both continuous and batch processes, enabling particle sizes <10–50 μm with higher throughput (~3 times and ~9 times, respectively) than the previous report.[10] The result is aqueous hydrogel microparticle suspensions with acceptable flow properties and stability at ultra-high antibody concentrations. This work represents a significant advancement in antibody concentration, with the potential to enable subcutaneous delivery of most monoclonal antibody therapies with doses <10 mg kg^{-1} for typical patient populations within a 2 mL volume constraint, while establishing a path towards scale-up.[15]

Materials and methods

Materials

Lyophilized total human IgG was purchased from Equitech-Bio, Inc (SLH56, Lot #25013-0256). Poly(ethylene)glycol (PEG, 3350 kDa) was purchased from Rigaku Reagents. Sodium alginate (5–40 cP) was purchased from Sigma. All other chemicals were purchased from Sigma and used without further purification.

Single-droplet dehydration

To examine the dehydration of single antibody droplets under various conditions, single-droplet dehydration experiments were conducted using the setup described in a previous work.[10] The IgG concentration of the antibody solution was held at 60 mg mL^{-1} while the PEG concentration was varied between 0.4–2% w/v (buffered at 5 mM HEPES, pH 7.4). Sodium alginate was also present in the solution at 0.2% w/v. Droplets were expelled from a syringe with a 30 G stainless steel needle (I.D. = 159 μm, O.D. = 312 μm) into a 1-pentanol (0.4% w/v Tween 80) reservoir. The dehydration of the droplet was recorded under a microscope and the change in droplet radius over time was analyzed using ImageJ. All experiments were performed at ambient temperature with an initial microdroplet radius between 100 and 150 μm (n = 3). The final particle loading and PEG concentration were calculated from the initial concentration and the final change in droplet size.

Antibody particle encapsulation in PEG solutions

To ensure the retention of the antibody solid phase in the aqueous storage solution, the apparent solubility of the amorphous solid antibody in suspension with PEG was evaluated. IgG ASD-laden alginate microparticles were generated *via* the solvent-based dehydration process, with an initial IgG concentration of 60 mg mL^{-1} and an initial PEG concentration of 0.6% w/v. The particle samples were transferred to a microcentrifuge tube and excess solvent was removed to adjust the total IgG content in each tube to 0.5 mg. 1 mL of storage buffer solution (5 mM HEPES, pH 7.4) with different % w/v concentrations of PEG was added each tube. The particles were equilibrated with the storage solution at room temperature (~22 °C). The antibody concentration in the supernatant was measured after 24 hours using 280 nm UV-vis absorbance (n = 3).

Continuous antibody particle production

Amorphous solid IgG-laden alginate microparticles were produced continuously using a microfluidic cross-junction (IDEX PEEK P-891, thru hole = 0.15 mm, O.D. = 1/16 in) with soft-walled tubing (PTFE, I.D. = 0.3 mm, O.D. = 1/16 in). The cross-junction consisted of three inlet ports and one outlet port. The dispersed phase, which was made up of aqueous IgG solution (60 mg mL^{-1}) with PEG (0.6% w/v), sodium alginate (0.2% w/v), and 5 mM HEPES (pH 7.4), was fed through one inlet. The continuous phase, water-saturated 1-pentanol with Tween 80 (0.4% w/v), was fed through the other two inlets perpendicular to the dispersed phase. The dispersed phase and continuous phase solutions were loaded into syringes on separate syringe pumps. The flow rate of the dispersed phase was set at 15 μL min^{-1}, and the flow rate of each continuous input was set at 600 μL min^{-1}. The produced droplets were collected at the outlet port and transferred to an unsaturated 1-pentanol bath with calcium chloride (0.01% w/v) and Tween 80 (0.4% w/v). Images of the droplets were taken immediately after collection, and after complete dehydration in the bath. The size distributions of the droplets and microparticles were analyzed using ImageJ (n > 50).

Batch antibody particle production

Amorphous solid IgG-laden alginate microparticles were produced *via* a batch emulsification process. The same dispersed phase as above was added dropwise to the water-saturated pentanol continuous phase (0.4% w/v Tween 80) in a 1 : 10 volume ratio (0.5 : 5 mL), with parallel batch processing. A magnetic stir bar was used to stir the mixture at a constant rate to produce droplets. The droplets were then transferred to an unsaturated 1-pentanol bath with calcium chloride (0.01% w/v) and Tween 80 (0.4% w/v) for solvent-based dehydration to produce the antibody-laden particles. Images of the droplets were taken before transferring to the bath, and after complete dehydration. The size distributions of the droplets and microparticles were analyzed using ImageJ (n > 50).

Scanning electron microscopy

The surface morphology of the dried solid antibody micrparticles was observed using high-resolution scanning electron microscopy (Zeiss HRSEM) at an accelerating voltage of 1 kV. Particle samples were prepared on SEM specimen stubs with double-sided carbon tape. To improve contrast in SEM imaging, the samples were coated with 1 layer of 5 nm gold nanoparticles.

Injection force measurements

The injectability of the antibody microparticle suspension was measured using injection force testing. Prior to characterization of the suspension, the suspension was mixed to ensure homogeneity and reduce particle settling and used immediately after mixing. The protocol described in a previous work was followed.[16] To measure injection force, a Zwick-Roell universal testing machine (model Z010) with a 500 N load cell and custom 3D-printed flat-plate compression attachment was used. The formulation was loaded into a plastic BD 1 mL syringe with a 25-gauge (ID = 260 μm, OD = 515 μm) Luer-lock needle. The syringe was held stationary by a clamp for the test duration. For each test, the stroke distance (displacement) was set at 25 mm, which corresponds to a ∼0.5 mL injection volume. The stroke speed was set at ∼1.4 mm s^{-1} so that it corresponds to a injection rate of 25 μL s^{-1}. All tests were performed at ambient conditions (n = 3). Images of the particle suspension prior to and following the injection test were captured under bright-field microscopy.

Size exclusion chromatography (SEC)

Analytical SEC was used to determine the quantity of IgG monomer and aggregates released from ASD-laden alginate microparticles. For this purpose, an Agilent 1200 HPLC instrument was used, with a TSKgel G3000SWXL (Tosoh Bioscience) analytical SEC column. SEC experiments were carried out at a flow rate of 0.4 mL min^{-1} in phosphate buffered saline (PBS) at pH 7.0. For the native control experiment, lyophilized IgG powder as received was dissolved into PBS and analyzed. Due to lot-to-lot variations in IgG quality, IgG from the same lot was used across all experiments (n = 3).

Fourier-transform infrared spectroscopy (FTIR)

IgG was analyzed in both the solvated and solid-state using FTIR-ATR spectroscopy (Thermo Fisher Nicolet is50). Either a 20 μL drop of IgG solution (60 mg mL^{-1}) in phosphate-buffered saline for solvated samples or a powder for solid-state samples was placed on the diamond ATR crystal. Solutions were filtered before measurement with a 0.2 μm filter. 256 scans were performed at 4 cm^{-1} resolution, with automatic background subtraction and atmospheric suppression. The spectra were analyzed in Fityk software. The amide I band region (1700–1600 cm^{-1}) was isolated, baseline-corrected, and area-normalized. Second derivative spectra of this region was obtained using 9-point Savitzky–Golay smoothing algorithm and peak-fitted with a Gaussian curve function and the Levenberg–Marquardt algorithm. Peaks were assigned to secondary structure components following literature conventions.[17,18] The relative areas of the fitted peaks were used for the quantification of IgG secondary structure (n = 3).

Circular dichroism (CD)

To determine IgG secondary structure, far-UV circular dichroism (CD) was used. IgG samples were prepared at 0.3–0.5 mg mL^{-1} in aqueous solution (10 mM phosphate buffer, pH 7.4), and spectra were obtained in a 1 mm quartz cuvette (Hellma Analytics) at ambient conditions with a JASCO J-1500 spectropolarimeter. The wavelength was scanned from 250–190 nm with a 0.5 nm data pitch, 1 nm bandwidth, 4 s digital integration time, and 50 nm min^{-1} scanning speed. The instrument was purged with nitrogen gas for at least 5 min prior to recording measurements. The data was reported as mean residual ellipticity following the protocol in Kelly *et al.* (n = 5).[19]

Enzyme-linked immunosorbent assay (ELISA)

ELISA bioassays were performed to determine IgG antibody recovery using sandwich binding assays. Human IgG total kit (Invitrogen) was used for identifying IgG binding. The assay was carried out according to the manufacturer's procedure.[20] The standard calibration curve from the assay is available in the SI (Fig. S1). ELISA quantification was expressed as a fraction of the mass recovered over the initial mass of antibody in the sample (n = 3).

In vitro release assay

To evaluate release of the antibody from the microparticles, *in vitro* release assays were performed. In the assay, ∼20 μL of the antibody-laden microparticle aqueous suspension was injected into a 2 mL centrifuge tube with 1 mL of pre-warmed (37 °C) simulated body fluid (SBF). SBF was formulated to mimic the composition of the SC environment based on previous literature, with 7.996 g L^{-1} sodium chloride, 0.350 g L^{-1} sodium bicarbonate, 0.224 g L^{-1} potassium chloride, 0.228 g L^{-1} potassium phosphate dibasic trihydrate, 0.305 g L^{-1} magnesium chloride hexahydrate, 0.278 g L^{-1} calcium chloride, 0.071 g L^{-1} sodium sulfate, 6.057 g L^{-1} tris(hydroxymethyl) aminomethane, and 40 mL L^{-1} of 1 M hydrochloric acid.[21] At consistent time intervals, 200 μL of the supernatant was removed and the protein concentration of the sample was measured *via* 280 nm UV–vis absorbance. The removed volume was immediately replaced with fresh warmed SBF. The volume of the initial particle suspension for release was chosen such that the total antibody concentration in the release medium would be <10 mg mL^{-1}, ensuring the medium would not be saturated during the test period. Concentration measurements were taken in triplicate using multiple sample replicates (n = 3).

Results and discussion

Antibody microparticle formulation

In the solvent-based dehydration process, an antibody amorphous solid dispersion (ASD) is formed from PEG-induced precipitation. This necessarily occurs due to the increase in both antibody and PEG concentration during dehydration. PEG is widely known to induce phase separation in proteins due to steric exclusion of PEG from the protein surface that results in attractive depletion interactions and the formation of protein-rich and protein-poor phases.[22] This phase transition is dependent on both protein and PEG concentration, with lower con-

centrations generally resulting in liquid–liquid phase separation (LLPS) and higher concentrations resulting in solid precipitation.[23,24] At sufficient PEG concentrations, the ASD formed is stabilized in the solid state by the presence of PEG preventing resolubilization of the protein. Formulating the antibody as an ASD is advantageous as proteins tend to have better long-term stability and longer shelf-lives as solids.[25]

The solvent-based dehydration process was first observed on a single-droplet scale to optimize the formulation before any scale-up was performed. In this formulation, IgG was used as a model antibody as the majority of clinically-relevant antibodies are of an IgG type.[26] Droplets of solution containing IgG, PEG, and alginate, buffered at pH 7.4 by a minimal amount of HEPES, were formed in a pentanol bath, using a previously-validated experimental setup.[10] The concentrations of IgG and alginate were fixed at 60 mg mL^{-1} and 0.2% w/v, respectively, while PEG concentration was varied. As the aim of these experiments was to maximize the achievable particle loading while maintaining IgG in a solid state at equilibrium, a minimum PEG concentration of 0.4% w/v was chosen for the optimization study. Time-lapsed images of a single antibody droplet in pentanol are shown in Fig. 1a. At t = 0 min, the droplet is completely clear, as IgG is soluble in aqueous solution at the initially low PEG concentration. At t = 3 min, the droplet has visibly shrunk due to water diffusing from the droplet into the bath, and the local increase in PEG concentration induces phase separation of the antibody, as observed by the change in opacity within the droplet. By t = 10 min, continued dehydration of the droplet results in precipitation of the antibody into an ASD, forming a solid antibody-laden microparticle. As shown, the resulting particle is opaque, with a high sphericity due to the presence of Tween 80 in the pentanol bath.

The relative change in droplet radius was recorded over time for varying initial PEG concentration ($C_{PEG,0}$), shown in Fig. 1b. The kinetics of the dehydration process were consistent in the initial time period regardless of PEG concentration, fitting well to the Epstein–Plesset model for droplet dissolution.[27] Due to the presence of solutes, the solid particle plateaued to an equilibrium size once water had been extracted to the fullest extent. This equilibrium size was dependent on PEG concentration, as expected, but did not follow a directly proportional relationship. The final particle loading and PEG concentration in the particle was calculated using the initial concentrations and change in droplet size (Fig. 1c). The particle loading varied between 570 and 640 mg mL^{-1} for initial PEG concentrations 0.4–0.7% w/v, representing approximately an order of magnitude increase in IgG concentration. While we hypothesized that lower initial PEG concentrations would result in a higher particle loading due to the greater change in

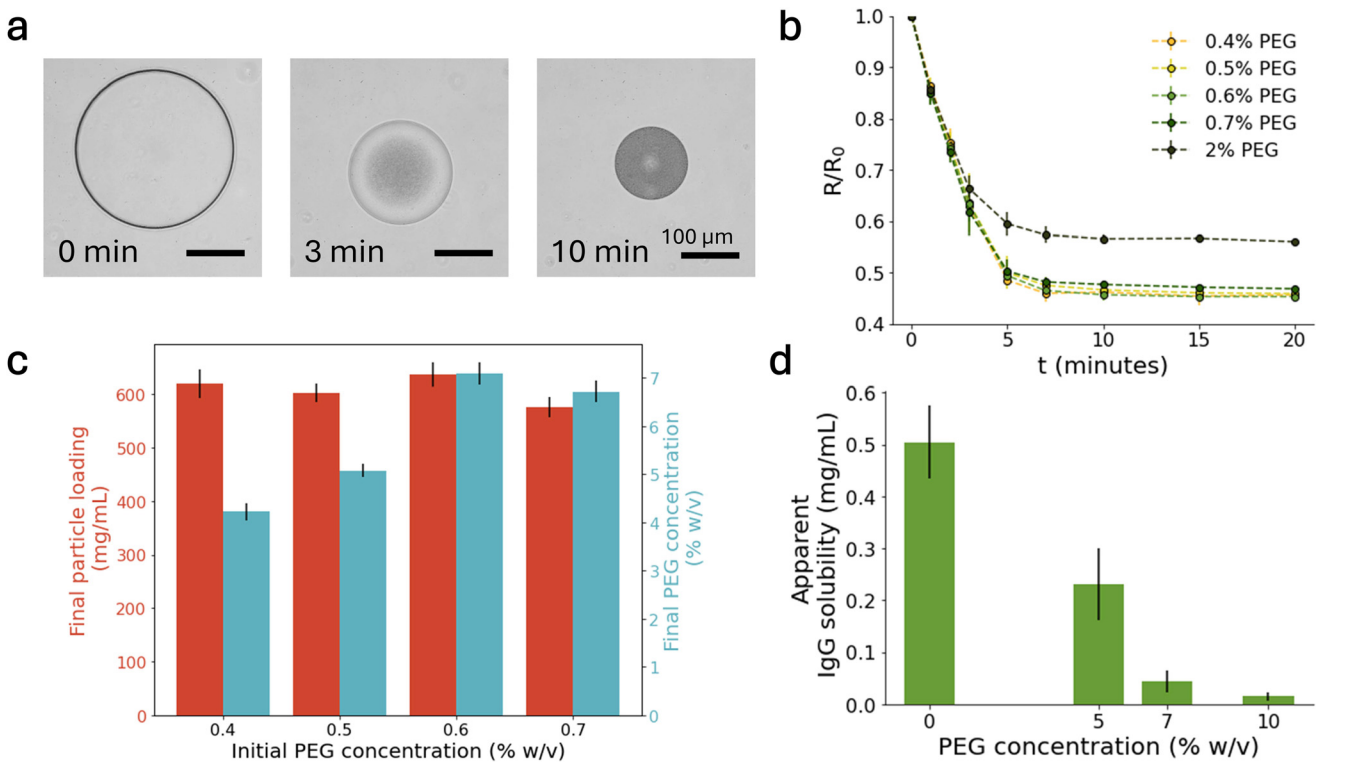

Fig. 1 (a) Time-lapse images of 60 mg mL^{-1} IgG, 0.6% PEG, 0.2% alginate in pentanol (0.4% w/v Tween 80, 0.01% w/v $CaCl_2$). (b) Change in scaled radius over time (min) for microparticles in pentanol with varying PEG concentration in the initial droplet. (c) Final particle loadings (mg mL^{-1}) and PEG concentrations (% w/v), calculated from the initial droplet IgG concentration, for varying initial PEG concentration. n = 3 for each condition. (d) Apparent solubility of IgG (mg mL^{-1}) from hydrogel microparticles in aqueous solutions of varying PEG concentration (% w/v), based on a total concentration of 0.5 mg mL^{-1}.

volume, this trend did not hold true, suggesting that solute concentration is not the only determinant of the equilibrium particle size and it is also dependent on other factors, such as ASD microstructure and packing and the effect of PEG on water activity.

Both the particle loading and final PEG concentration were maximized at $C_{PEG,0}$ = 0.6% w/v. This condition was optimal in that it resulted in the highest particle loading (637 ± 23 mg mL^{-1}), enabling ultra-high concentration particle formulations, as well as the highest PEG concentration for stabilizing IgG in the ASD form. The particle loading was confirmed *via* UV-vis absorbance to be 642 ± 9 mg mL^{-1} by dissolving the formulation in phosphate-buffered saline and measuring the supernatant concentration. The importance of PEG to maintain the solid state of IgG is shown in Fig. 1d, where the apparent solubility of IgG was measured in solutions of varying PEG concentration. Clearly, the solubility of IgG decreases with increasing PEG concentration, indicating that IgG is stabilized in the solid form at higher PEG concentrations. Particularly, there is a sharp decrease in apparent solubility between 5 and 7% w/v PEG. The low apparent solubility at ≥7% w/v PEG suggests that this is the minimum PEG concentration to form a stable ASD, which is indeed the case in the final particle composition starting from $C_{PEG,0}$ = 0.6% w/v. IgG within the particle was maintained as a solid at these conditions, which is important for ultra-high concentration formulations, as antibodies are more stable in the solid state rather than in solution.[28] This work refines the formulation by optimizing the particle loading and identifying the minimum PEG concentration for stabilizing the solid antibody, compared to the previous work where 15% w/v PEG was selected as a sufficient but not optimal concentration to precipitate and stabilize the ASD.[10] Given the apparent solubility results in Fig. 1d, 7% w/v PEG is revealed to be the minimum threshold at which IgG remains as a solid in the particle and thus selected as the storage buffer condition.

Microparticle production and characterization

Following the single-particle studies, the solvent-based dehydration process was carried out at a larger scale utilizing continuous microfluidic droplet generation, as described. The optimal formulation from the previous section was used as the canonical formulation for the dispersed phase. In the first step of the process, droplets containing IgG, PEG, and alginate were generated *via* pinch-off at a microfluidic cross-junction with a water-saturated pentanol continuous phase. Dehydration and cross-linking of the droplets was accomplished in the second step when the droplets were transferred to an unsaturated pentanol bath with calcium chloride. Through these two steps, droplet dehydration was decoupled from droplet generation which prevents clogging in the microfluidic system and allowed for higher flow rates (~3 times higher compared to previous work).[10] In both steps, Tween 80 was present in the continuous phase to control the interfacial tension and limit particle aggregation. Size distributions of the droplets and the dehydrated particles are shown in Fig. 2a. With the microfluidic method, droplets with an average diameter of 95 μm were generated. Cross-flow microfluidics is a well-characterized method to continuously form droplets suspended in a second liquid phase with a controlled size distribution in the range of 10–100 μm.[29] The droplet size produced by a cross-junction is influenced by the junction thru-hole size, interfacial tension between the dispersed and continuous phases, as well as the relative and absolute flow rates of the two phases. In this case, the flow rate ratio Q_d/Q_c was chosen to be 40, based on the results of a previous study, and the dispersed flow rate was set at the maximum which could be attained by the syringe pumps, to allow for efficient droplet generation. Once dehydrated, the particles had an average diameter of 32 μm, the decrease in size corresponding to the removal of water from the droplet. Both the droplet and particle size distributions had PDI <0.2, indicating that the distributions were relatively monodisperse before and after dehydration. However, it is noted that the particle PDI is higher than the droplet PDI, which suggests that droplet-to-droplet size differences are enhanced upon dehydration. The broadening of the size distribution of the particles is consistent with previous studies of droplet solvent extraction and is due to local concentration differences which occur during drying.[30] These local differences are also responsible for the dimpled structures displayed in some particles, with dimpled particles making up ~5–10% of the particle population (Fig. 2c and d).[31]

Fig. 2e shows a magnified image of a single dried ASD-laden microparticle, where the ASD microstructure can be observed. In comparison, Fig. 2f shows an image of a bulk IgG ASD at similar conditions to the particle. The ASD microstructure in both images have comparable feature sizes, signifying the effective ASD formation and encapsulation of the microfluidic solvent-based dehydration process. Fig. 2g and h are representative scans captured from scanning electron microscopy of the dried microparticles. Though the microstructure of the ASD has a characteristic texture, the microparticle itself has a smooth surface, likely due to the presence of the alginate hydrogel encapsulating the ASD, which masks the protein at the surface. Moreover, the particles maintain a round and spherical shape when dried, indicating that dehydration of the droplets was relatively consistent. Due to the flow rate and geometrical limitations of the cross-flow microfluidics system, a batch microparticle production process was performed to demonstrate the generation of microparticles at a wide range of particle sizes.[32] The ability to produce particles at varying size distributions may be of interest for various clinical applications, towards a more adaptable formulation platform. The decoupling of droplet generation from droplet dehydration in two steps enabled a variety of particle production processes, including the batch process described in this work. Droplets of the dispersed phase antibody solution were generated *via* batch emulsification in a water-saturated pentanol continuous phase. This process can be scaled up by phase volumes or parallelized at the bench-scale to increase throughput. At the volumes processed for this work, the batch process was ~3–9 times higher in throughput compared to using microfluidics. On the bench-scale, the current process con-

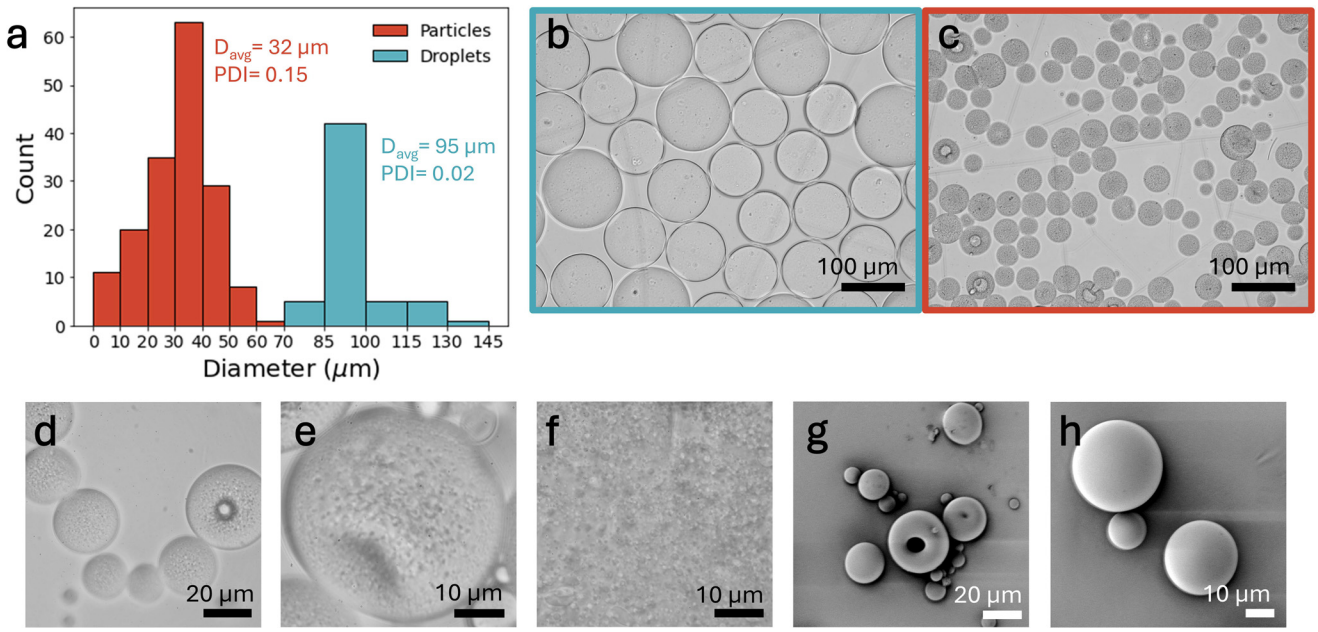

Fig. 2 (a) Size distributions of droplets (blue) and particles (red) produced from microfluidic emulsification. (b) Optical microscope image of droplets produced *via* microfluidic emulsification. (c) Optical microscope image of particles produced *via* solvent-based dehydration of microfluidic-produced droplets. (d and e) Magnified optical microscope images of dehydrated antibody-laden hydrogel particles. (f) Microscope image of IgG amorphous solid dispersion (ASD) with 7% w/v PEG. (g and h) Scanning electron microscope (SEM) images of dehydrated antibody-laden hydrogel particles.

ducted in 50 mL (0.05 L) vessels results in a g per day output. In order to enable kg per day production, scale-up to 50 L vessels could be carried out at a pilot-scale, representing the next step in demonstrating the potential for this process for clinical application.

The diameter of the droplets was controlled by varying the stirring rate during emulsification (Fig. 3a). As with the continuous method, the droplets were then transferred to an unsaturated pentanol bath with calcium chloride, where particles were produced *via* solvent-based dehydration. Representative images of droplets and particles produced *via* batch emulsification are shown in Fig. 3b and c. The size of the particles was set by the initial size of the droplets, with average diameters ranging between 7 µm and 50 µm for the conditions tested here. Particle size distribution of droplets and the dehydrated particles are shown in Fig. 3d and e for 1000 rpm and 1750 rpm stirring rates, respectively. Because the particle size in this batch emulsification process is dependent on the stirring rate, much smaller particles were able to be produced using this batch process compared to the microfluidic process, which would require extremely high flow rates in microfluidics that are not viable. Other emulsification methods, such as ultrasonication or high-pressure homogenization, may have alternate parameter optimizations to control particle size resulting from those processes. The production of particles with diameter <10 µm with this batch process represents an advancement over the previous microfluidic process, particularly for subcutaneous injection where thinner needles may require smaller particles for suitable injectability.[33]

After the solvent-based dehydration process, the microparticles were separated from the solvent *via* centrifugation, followed by solvent removal and resuspension of the particles in a PEG 3350 solution (7% w/v). This allows for the particles to be delivered as a solid suspension in an aqueous carrier. The delivery of the particles in an aqueous vehicle is preferable to non-aqueous carriers, which have increased injection pain, toxicity, as well as manufacturing challenges and regulatory burdens.[34–36] Importantly, the PEG concentration in the suspension was selected to be the minimum which could stabilize the ASD, enabled by a systematic characterization of apparent IgG solubility in various PEG solutions. At higher PEG concentrations, the viscosity of the PEG solution could negatively affect the flow properties of the suspension, and lead to adverse effects such as cytotoxicity, though PEG 3350 has been shown to be tolerated in subcutaneous injection at up to 10% w/v.[37,38] To assess the formulation's flowability, injection force tests were conducted on the final aqueous particle suspension. Compared to other rheological properties, injection force is the most clinically relevant measurement, with quantitative results that can be easily translated for clinical applications.[39] Injection force is a key concern, as injectability is typically where high-concentration formulations fail to meet clinical standards due to the increased viscosity.[6] For ultra-high concentrations formulations, lower injection forces are necessary to enable administration of the injections.[7]

To perform the injection force tests, the particle suspension was loaded into a syringe. Using an universal mechanical testing machine, a downward compressive force was applied

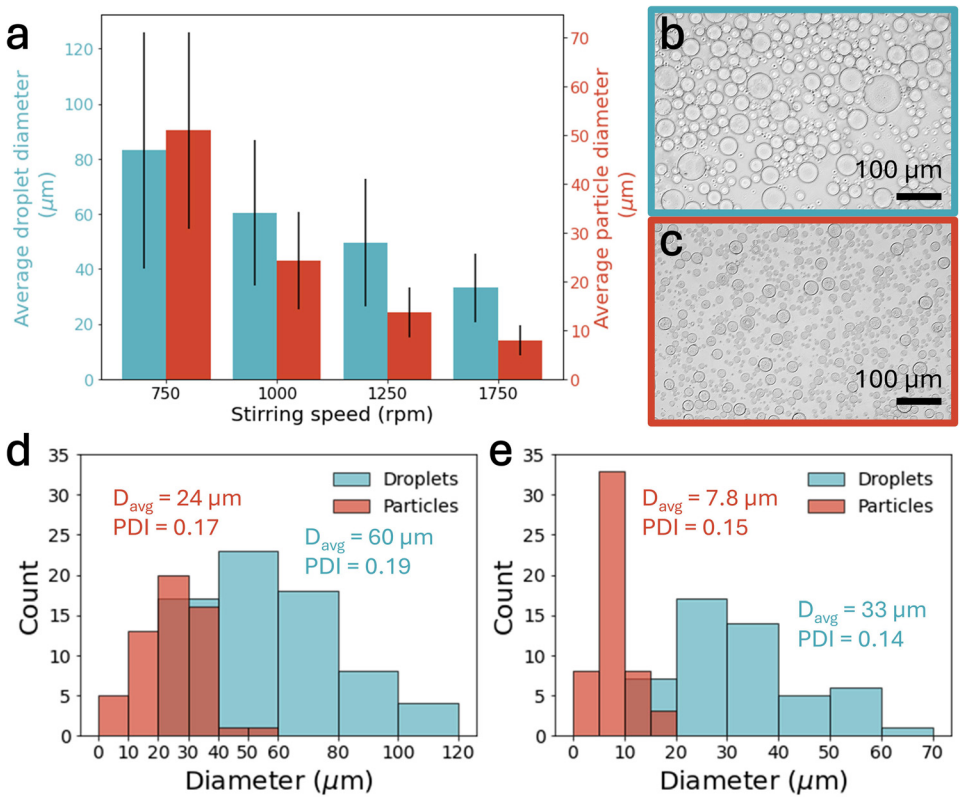

Fig. 3 (a) Average droplet and particle diameters (μm) produced from batch emulsification at varying stirring rates (rpm). (b) Optical microscope image of droplets produced *via* batch emulsification at 1000 rpm. (c) Optical microscope image of particles produced *via* solvent-based dehydration of batch-produced droplets. Size distributions of droplets (blue) and particles (red) produced from batch emulsification at (d) 1000 rpm and (e) 1750 rpm stirring rate.

onto the syringe plunger over a specified displacement. The particle formulations tested consisted of particles made from the continuous process (D_{avg} = 32 μm) as well as particles made from the batch process at two different stirring rates (D_{avg} = 24 μm and D_{avg} = 7.8 μm). Formulation concentrations (C_{form}) were first estimated based on the previously calculated particle loading and a particle volume fraction ($V_{particles}/V_{particles+PEG\ solution}$) of ≈0.7–0.75 in a 7% w/v PEG solution. The particle volume fraction was approximated by centrifuging a known volume of a dilute particle suspension and removing an appropriate amount of supernatant to achieve the desired particle volume fraction. A relatively high particle volume fraction was possible due to the softness and deformability of the hydrogel particles. The soft particles allow for closer packing than the theoretical hard-sphere limit, with other reports of similar hydrogel microparticle suspensions achieving particle volume fractions greater than 0.80 to 1.0.[9,40]

For each formulation, C_{form} were then measured directly, using the UV-vis absorbance method for samples diluted 1 : 20 in phosphate-buffered saline. The presence of alginate in these samples was not found to interfere with the measurement of antibody concentration from UV-vis (SI, Fig. S2). The continuous-produced formulation had a concentration (C_{form}) of 450 ± 6 mg mL^{-1} while the batch-produced formulation had C_{form} = 480 ± 7 mg mL^{-1}. While similar previously developed formulations were limited to <400 mg mL^{-1}, optimization of PEG concentration and ASD packing in the particle has enabled ultra-high concentration formulations. This increase in concentration is a significant advancement for SC administration, as many immune-related conditions require high doses (>30–50 mg kg^{-1}).[5] Ultra-high concentration formulations allow these therapies to be delivered in lower volumes or less injections, which is conducive to accessibility and patient compliance.[5,14] In the injection force test, a standard SC 25-gauge needle was used, and a flow rate of 25 μL s^{-1} was selected as a clinically relevant injection speed, corresponding to a 0.5 mL dose injected in 20 seconds. The average injection force over the syringe plunger displacement is shown in Fig. 4a for the various formulations. From the beginning of the test, all of the microparticle suspensions experience a start-up regime, where the injection force steadily increases until it plateaus, which is commonly observed in injection force testing.

The injection force between tests tends to be more variable in the start-up regime, likely due to differences in particle distribution within the syringe.[39] However, the injection force in the plateau regime is relatively consistent and can be averaged to obtain the glide force, which was between 15 and 20 N for

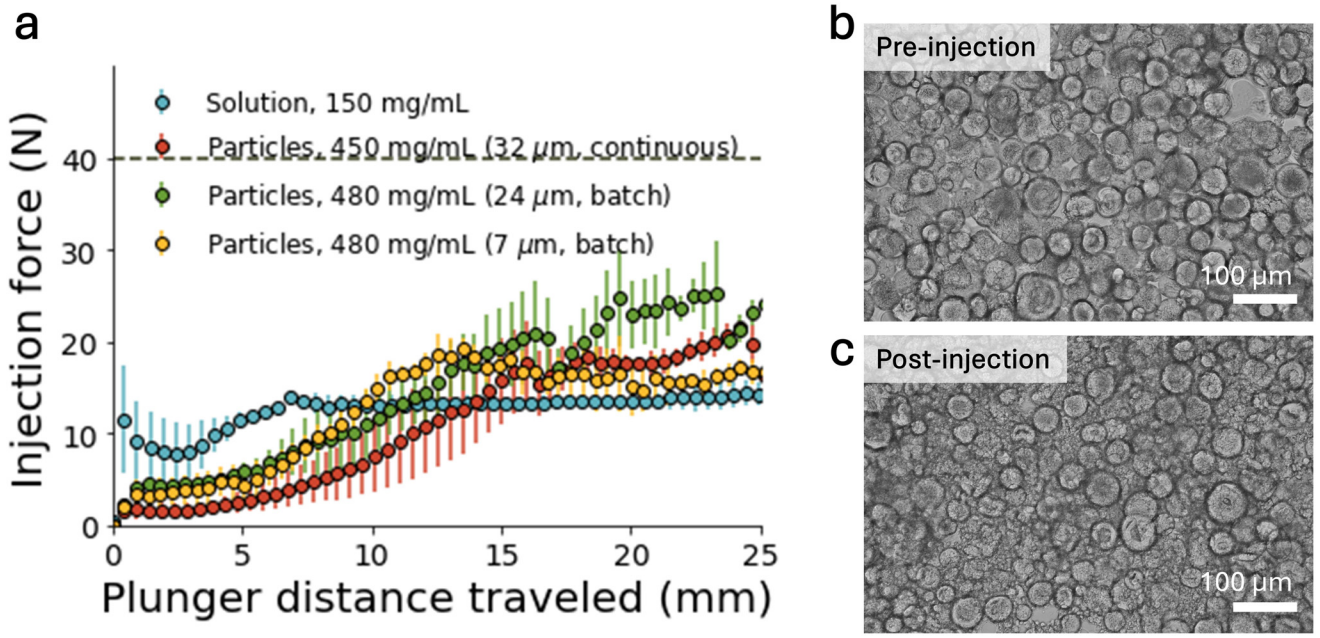

Fig. 4 (a) Injection force (N) *versus* plunger distance traveled (mm) for an IgG solution control, reproduced from ref. 10 (blue), microparticle suspension produced by continuous microfluidics (red), microparticle suspension produced by batch emulsification at 1000 rpm (green), and microparticle suspension produced by batch emulsification at 1750 rpm (yellow). (b) Optical microscope image of microparticle suspension produced by continuous microfluidics before performing injection force test. (c) Optical microscope image of microparticle suspension produced by continuous microfluidics after performing injection force test.

each test for the continuous-produced particles (mean = 17.8 N). This glide force is comparable to injection forces reported for other ultra-high concentration formulations and is well-below the recommended limit of 40 N for SC administration.[13,41,42] The same mean glide forces for the batch-produced formulations were 21.4 and 16.5 N for the larger and smaller particle sizes, respectively. Out of the three particle suspensions, the smallest particles (D_{avg} = 7.8 μm) had the lowest mean glide force, which was expected as smaller particle sizes generally improve injectability.[43] In addition, the same tests for a plain IgG solution (150 mg mL^{-1}) resulted in comparable glide forces as the microparticle suspension, even though the suspension was ≥3 times greater in concentration than the solution. Microscope images of the continuous-produced particles pre- and post-injection are shown in Fig. 4b and c, respectively. These images show that the particles remain intact and relatively undeformed during the injection process. The alginate hydrogel encapsulating the ASD lends softness and deformability to the microparticles, allowing them to retain their shape under shear stress. In addition, the needle gauge size was ~8× the average diameter of the largest tested particles, which is significantly higher than the recommended 3–4× for syringeability.[44] The hydrogel microparticles, which are not only deformable but also shear-thinning and lubricious, contribute to the relatively low injection forces of the suspension, allowing the antibodies to be readily delivered at ultra-high concentrations. This is a significant result for SC applications, as the potential for self-administration and home-based care depends upon the patient's ability to comfortably perform the injection.[45] Here, we show that the particle suspension can be delivered at an ultra-high concentration of 480 mg mL^{-1} with acceptable injection forces. Thus, our formulation is suitable for SC self-administration, granting the benefits of accessibility, patient compliance, and improved quality-of-life.

Antibody characterization

To ensure the quality and stability of the antibody encapsulated in the hydrogel microparticles *via* the solvent-based dehydration process, we performed extensive characterization of the antibody. Size-exclusion chromatography (SEC) was performed to show that no irreversible aggregation had occurred during dehydration. In Fig. 5a, the UV traces of native IgG and IgG released from the particles in suspension immediately after formulation and after 4 months of storage in 7% w/v PEG solution at 4 °C are shown. It is useful to compare the traces relative to the native antibody as its quality is dependent on the source material and can vary based on the supplier and the manufacturing lot. Additional SEC data is available in the SI regarding lot-to-lot variation of antibody quality (SI, Fig. S3a). The traces of native and released IgG displayed similar peaks and had similar monomer percentages, indicating that the quality of IgG was retained when formulated in the microparticle suspension. The quality of released IgG is also independent of particle size and production method (SI, Fig. S3b). In addition, the monomer percentage remained stable over a period of 4 months with minimal aggregation during storage, and leaching of antibody from the sample as

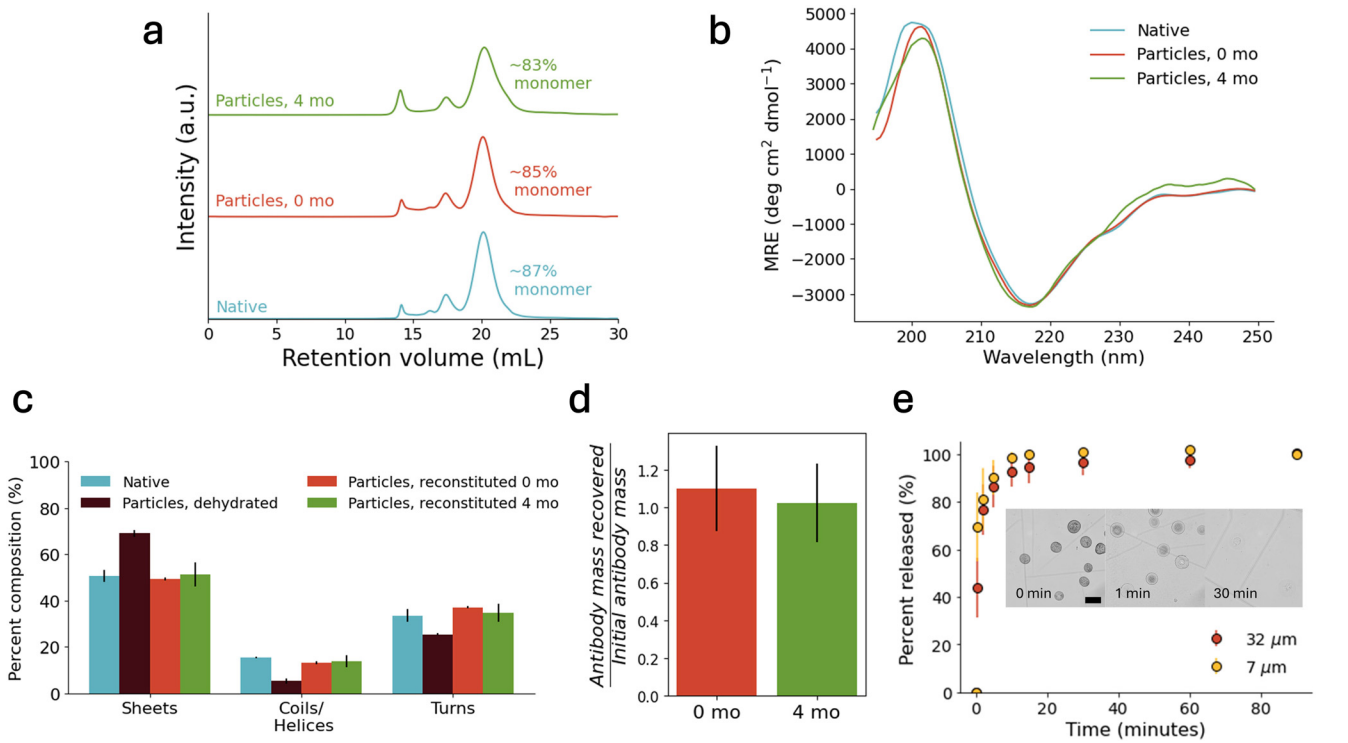

Fig. 5 (a) UV traces from size exclusion chromatography of IgG from native control sample (blue) and IgG released from microparticles after 0 months (red) and 4 months of storage in suspension (green). (b) Mean residual ellipticity (deg cm^2 dmol^{-1}) from circular dichroism measurements of native IgG control (blue) and IgG released from microparticles immediately after formulation (red) and after 4 months of storage in suspension (green). (c) Secondary structure composition as calculated from FTIR measurements for native IgG control (blue), dehydrated IgG particles (brown), and IgG reconstituted immediately after formulation (red) and after 4 months of storage in suspension (green). (d) Antibody mass recovery results from ELISA for IgG from microparticles, released immediately after formulation (0 months) and after 4 months of storage in suspension. (e) Kinetic release profile for IgG released from hydrogel microparticles, with mean diameter of 32 μm (red) and 7 μm (yellow), in simulated body fluid (SBF) at 37 °C. Time-lapse images of ASD-laden hydrogel microparticles in SBF are inset as a demonstration (scale bar = 50 μm).

measured by UV-vis absorbance was minimal (<2 mg mL^{-1}, ~99% encapsulated). As antibodies are susceptible to aggregation as concentration increases, the recovery of monomeric IgG from the particles here suggests that the process is suitable for formulating stable IgG at ultra-high concentrations.[4]

Characterization of the antibody's secondary structure was also performed to study its stability in the formulation. As the crowding of proteins at high concentrations lead to intermolecular interactions which can perturb protein structure, confirming structural stability is crucial to quality control for ultra-high concentration formulations.[46,47] Following production of the ASD-laden hydrogel microparticles, IgG was released from the particles in suspension into solution for analysis. Fig. 5b shows the mean residual ellipticity (MRE) of native and released IgG from far-UV circular dichroism (CD) spectroscopy. Given the parity of the MRE values between the native and released conditions, we could conclude that the dehydration–encapsulation process did not irreversibly affect the structure and conformation of the antibody. However, as quantification can be difficult to achieve with CD spectroscopy, Fourier-transform infrared (FTIR) spectroscopy was used to quantify the secondary structural composition, *via* deconvolution and analysis of the amide I band region (1700–1600 cm^{-1}).[17,48] Fig. 5c shows the estimated composition from FTIR of native IgG, dehydrated particles, and IgG reconstituted (*i.e.* released) from the particles in suspension. The comparison of the dehydrated IgG particles and reconstituted IgG highlights the importance of resuspending the particles in aqueous solution following dehydration. Both the native and reconstituted IgG showed a β-sheet dominant structure (~50%), which is common for immunoglobulin antibodies, usually ranging between 40–60% of the total secondary structure.[49,50] The other secondary structural features, β-turns (~35%) and random coils/α-helices (~15%), were also in the range of previous literature.[50,51] There were no significant differences between the native and reconstituted IgG compositions, and the IgG secondary structure does not show any changes when reconstituted 4 months after storage in the suspension formulation, which is consistent with the CD spectroscopy analysis. On the other hand, IgG in the dehydrated particles which were not reconstituted, showed significantly more β-sheet features (~70%) compared to the native structure. The increase in β-sheet composition is typical for dehydration-induced aggregation, when the structures are perturbed due to the removal of water and rearrangement of intermolecular interactions.[52,53] However, these changes were shown to be

reversible upon dissolution of the antibody in an aqueous medium, as the reconstituted IgG recovers its native structure. This result is consistent with previous reports of proteins reversing their dehydration-induced structural changes upon rehydration.[10,54] Importantly, we demonstrated conservation of the antibody's structural integrity at an ultra-high concentration, with any changes reversible upon reconstitution in an aqueous environment.

ELISA assay was performed to assess the structural integrity for IgG released from the particles immediately following formulation and after 4 months of storage as a microparticle suspension. Fig. 5d shows that the antibody is fully recovered from the sample at both 0 months and 4 months. The fractional mass recovery of the released IgG is within the acceptable recovery range for immunoassays of 80–120% and demonstrates no loss of structural integrity from the antibody in the particle formulation.[55] In this formulation process, the antibody remained structurally stable as a PEG-stabilized ASD in the microparticle suspension over months post-processing, even when formulated at an ultra-high concentration. The robust characterization performed in this work supports the viability of this new formulation to be used for clinical applications, in order to improve the delivery of antibodies and immunotherapies *via* SC administration.

Finally, *in vitro* release assays were conducted to demonstrate that the antibody could be easily released from the microparticle suspension, upon injection into a physiological medium. In these assays, the microparticle suspension was injected into simulated body fluid (SBF), which mimics the ionic composition of subcutaneous fluid, at body temperature (37 °C).[21] The release profiles for IgG from particles of two different size distributions are shown in Fig. 5e, inset with qualitative visualization of the release of IgG from multiple microparticles immersed in SBF by observing a decrease in the opacity of the particles over time. Initially, IgG is present as a solid ASD in the hydrogel particles, due to the presence of PEG in the suspension. Upon injection into SBF, the suspension is dispersed, and the local PEG concentration decreases, thus prompting the antibody to dissolve, as the PEG concentration is too low to stabilize the ASD. The dissolved antibody will then diffuse from the particle, leaving behind the blank alginate scaffold. Release from the particle is rapid, with >80% of the antibody being released within the first 5 minutes of the assay. Such fast release, termed as 'burst-release', is characteristic of hydrogel-based delivery systems, as water permeates quickly through the hydrogel network and causes the drug cargo to be released. The kinetics of antibody release are faster in the smaller particle size, with 68% of the antibody released in the first 30 seconds compared to 43% for the larger particle size, which is expected as the smaller particles have a higher surface area-to-volume ratio which enables the faster diffusion of antibody from the particle. The release profiles shown here are similar to previously reported high-concentration antibody formulations, with characteristic burst release but faster release kinetics owing to the smaller particle size here compared to previous formulations.[9,10] However, regardless of particle size, complete release of IgG was achieved, indicating that the antibody is not constrained within the particles when exposed to a physiological environment, for the purposes of an efficient and effective dose. Overall, we show that our ultra-high concentration particle suspension has acceptable quality, stability, and release properties, positioning our formulation as feasible for SC applications in expanding the delivery options for antibody therapeutics.

Conclusions

This work expands upon previous developments in high-concentration antibody formulation by applying a solvent-based dehydration platform and identifying an optimized formulation. The platform was also expanded by demonstrating an alternative batch particle production process to enable the formation of particles <10 μm in diameter. The improvements to the formulation process resulted in an ultra-high concentration antibody microparticle suspension that was shown to be injectable and stable over a period of 4 months at up to 480 mg mL^{-1}. The marked increase in antibody concentration compared to previous formulations below 400 mg mL^{-1} is significant for enabling SC delivery of immunotherapies. As an example in practical terms, a 60 kg patient requiring an 8 mg kg^{-1} dose that is typical of an oncology-related antibody therapy, the ultra-high concentration formulation could be delivered in a single 1 mL injection, resulting in significant reductions in patient burden and treatment costs.[56] This work is an advancement towards at-home treatments for cancer and other conditions, reduced healthcare costs, and a more accessible therapeutic landscape. We build upon prior work to show that this formulation platform yields viable and clinically relevant antibody particle suspensions for SC injection. Further studies investigating the long-term shelf-life, room-temperature stability, as well as *in vivo* bioavailability and biocompatibility and injectability testing with pre-filled syringes and auto-injectors should be performed for translating these formulations to the clinic.

Author contributions

Talia Zheng: conceptualization, data curation, formal analysis, investigation, methodology, visualization, and writing (original draft). Patrick S. Doyle: conceptualization, funding acquisition, project administration, resources, supervision, validation, and writing (review & editing).

Conflicts of interest

A provisional patent application based on prior work related to this study has been filed by Massachusetts Institute of Technology (MIT), on which T. Z. and P. S. D. are listed as inventors.

Data availability

No standardized datatype data were generated in this study. This study did not generate new code. Any additional information required to reanalyze the data reported in this paper is available from the corresponding author.

Supplementary information (SI) is available. See DOI: https://doi.org/10.1039/d6pm00199h.

Acknowledgements

The authors thank Dr Allan S. Myerson and Dr Hadley Sikes for their assistance in SEC-HPLC and ELISA characterization. This work was carried out in part through the use of facilities at MIT.nano, MIT Biophysical Instrumentation Facility, and the Institute of Soldier Nanotechnologies. This material is based upon work supported by the Massachusetts Institute of Technology Office of Graduate Education and the Robert T. Haslam (1911) chair to PSD.

References

1 M. S. Castelli, P. McGonigle and P. J. Hornby, *Pharmacol. Res. Perspect.*, 2019, **7**, e00535.
2 G. Jacquot, P. Lopez Navarro, C. Grange, L. Boudali, S. Harlepp, X. Pivot and A. Detappe, *Adv. Mater.*, 2024, **36**, 2406604.
3 A. C. Anselmo, Y. Gokarn and S. Mitragotri, *Nat. Rev. Drug Discovery*, 2019, **18**, 19–40.
4 J. Zarzar, T. Khan, M. Bhagawati, B. Weiche, J. Sydow-Andersen and S. Alavattam, *mAbs*, 2023, **15**, 2211185.
5 I. Ghosh, H. Gutka, M. E. Krause, R. Clemens and R. S. Kashi, *mAbs*, 2023, **15**, 2205540.
6 M. Desai, A. Kundu, M. Hageman, H. Lou, S. Tenjarla, C. C. Sun, F. Zhang and O. Rahman, *AAPS J.*, 2025, **27**, 142.
7 L. R. R. Mijangos, S. E. Harding and N. J. Darton, *Biophys. Rev.*, 2025, **17**, 1013–1031.
8 A. Erfani, J. M. Schierferstein, P. Reichert, C. N. Narasimhan, C. Pastuskovas, V. Parab, D. Simmons, X. Yang, A. Shanker, P. Hammond and P. S. Doyle, *Adv. Healthcare Mater.*, 2023, **12**, 2202370.
9 A. Erfani, P. Reichert, C. N. Narasimhan and P. S. Doyle, *iScience*, 2023, **26**, 107452.
10 T. Zheng, L. Attia, J. Teng and P. S. Doyle, *Adv. Mater.*, 2026, **38**, e16429.
11 J. M. Schieferstein, P. Reichert, C. N. Narasimham, X. Yang and P. S. Doyle, *Adv. Ther.*, 2021, **4**, 2000216.
12 C. Marschall, M. Witt, B. Hauptmeier and W. Frieß, *J. Pharm. Sci.*, 2022, **111**, 861–867.
13 C. K. Jons, A. N. Prossnitz, N. Eckman, C. Dong, A. Utz and E. A. Appel, *Sci. Transl. Med.*, 2025, **17**, eadv6427.
14 S. Shadbar, L. Liu, Y. Tang, F. Kabir, S. Vartak, Z. Gui, M. Huck, E. Weinstein, M. Khwaja, A. Dehadrai, T. Carter, J. Ivey, C. Sudrik, P. Brown, L. Charles and D. Dadon, *Drug Delivery Transl. Res.*, 2026, **16**, 202–215.
15 J. T. Ryman and B. Meibohm, *CPT: Pharmacometrics Syst. Pharmacol.*, 2017, **6**, 576–588.
16 T. Zheng and P. S. Doyle, *RSC Pharm.*, 2025, **2**, 186–196.
17 S. Matheus, W. Friess and H.-C. Mahler, *Pharm. Res.*, 2006, **23**, 1350–1363.
18 J. Kong and S. Yu, *Acta Biochim. Biophys. Sin.*, 2007, **39**, 549–559.
19 S. M. Kelly, T. J. Jess and N. C. Price, *Biochim. Biophys. Acta, Proteins Proteomics*, 2005, **1751**, 119–139.
20 Thermo Fisher Scientific, *Human IgG Total ELISA Kit*, 2019.
21 M. R. C. Marques, R. Loebenberg and M. Almukainzi, *Dissolution Technol.*, 2011, **18**, 15–28.
22 M. d. C. Pons Royo and A. Jungbauer, *Prep. Biochem. Biotechnol.*, 2025, **55**, 935–954.
23 D. Atha and K. Ingham, *J. Biol. Chem.*, 1981, **256**, 12108–12117.
24 N. Rakel, L. Galm, K. C. Bauer and J. Hubbuch, *Biotechnol. Prog.*, 2015, **31**, 145–153.
25 L. L. Chang and M. J. Pikal, *J. Pharm. Sci.*, 2009, **98**, 2886–2908.
26 W. R. Strohl, *Antib. Ther.*, 2024, **7**, 132–156.
27 P. S. Epstein and M. S. Plesset, *J. Chem. Phys.*, 1950, **18**, 1505–1509.
28 Y. Zhang, D. A. Davis, K. AboulFotouh, J. Wang, D. Williams, A. Bhambhani, M. Zakrewsky, M. Maniruzzaman, Z. Cui and R. O. Williams III, *Adv. Drug Delivery Rev.*, 2021, **172**, 183–210.
29 G. F. Christopher and S. L. Anna, *J. Phys. D: Appl. Phys.*, 2007, **40**, R319–R336.
30 T. Watanabe, C. G. Lopez, J. F. Douglas, T. Ono and J. T. Cabral, *Langmuir*, 2014, **30**, 2470–2479.
31 W. N. Sharratt, A. Brooker, E. S. J. Robles and J. T. Cabral, *Soft Matter*, 2018, **14**, 4453–4463.
32 S. S. Aboelela, M. Ibrahim, A. Z. M. Badruddoza, V. Tran, J. K. Ferri and T. D. Roper, *Int. J. Pharm.*, 2021, **606**, 120906.
33 M. Sarmadi, A. M. Behrens, K. J. McHugh, H. T. Contreras, Z. L. Tochka, X. Lu, R. Langer and A. Jaklenec, *Sci. Adv.*, 2020, **6**, eabb6594.
34 R. G. Strickley, *Pharm. Res.*, 2004, **21**, 201–230.
35 C. Marschall, M. Witt, B. Hauptmeier and W. Frieß, *J. Pharm. Sci.*, 2023, **112**, 61–75.
36 C. Marschall, M. Witt, B. Hauptmeier and W. Friess, *Eur. J. Pharm. Biopharm.*, 2021, **161**, 37–49.
37 H. Pham Le Khanh, D. Nemes, Á. Rusznyák, Z. Ujhelyi, P. Fehér, F. Fenyvesi, J. Váradi, M. Vecsernyés and I. Bácskay, *Polymers*, 2022, **14**, 279.
38 M. X. Yang, B. Shenoy, M. Disttler, R. Patel, M. McGrath, S. Pechenov and A. L. Margolin, *Proc. Natl. Acad. Sci. U. S. A.*, 2003, **100**, 6934–6939.
39 M. H. Chen, L. L. Wang, J. J. Chung, Y.-H. Kim, P. Atluri and J. A. Burdick, *ACS Biomater. Sci. Eng.*, 2017, **3**, 3146–3160.
40 H. M. Shewan and J. R. Stokes, *J. Colloid Interfacial Sci.*, 2015, **442**, 75–81.

41 J. Yadav, S. Uddin, F. Civati, W. Ma, A. Liebminger, W. Teschner, G. André, B. L. Trout, R. D. Braatz and A. S. Myerson, *J. Pharm. Sci.*, 2025, **114**, 1605–1614.
42 R. P. Watt, H. Khatri and A. R. G. Dibble, *Int. J. Pharm.*, 2019, **554**, 376–386.
43 C. Zhao, Z. Zhu, X. Cao, F. Pan, F. Li, M. Xue, Y. Guo, Y. Zhao, J. Zeng, Y. Liu, Z. Yang, Y. Liu, F. Ren and L. Feng, *Eur. J. Pharm. Biopharm.*, 2023, **190**, 58–72.
44 M. A. Whitaker, P. Langston, A. Naylor, B. J. Azzopardi and S. M. Howdle, *J. Mater. Sci.: Mater. Med.*, 2011, **22**, 1975–1983.
45 M. Puccetti, M. Pariano, A. Schoubben, S. Giovagnoli and M. Ricci, *Pharmacol. Res.*, 2024, **201**, 107086.
46 G. V. Barnett, W. Qi, S. Amin, E. N. Lewis, V. I. Razinkov, B. A. Kerwin, Y. Liu and C. J. Roberts, *J. Phys. Chem. B*, 2015, **119**, 15150–15163.
47 A. Yamane, T. Oyama, K. Tamura, M. Kanno, S. Norimoto, F. Kohl, S. Suzuki and K. Akao, *Biophys. J.*, 2022, **121**, 42a.
48 V. Joshi, T. Shivach, N. Yadav and A. S. Rathore, *Anal. Chem.*, 2014, **86**, 11606–11613.
49 C. E. Giacomelli, M. G. Bremer and W. Norde, *J. Colloid Interface Sci.*, 1999, **220**, 13–23.
50 A. Janda and A. Casadevall, *Mol. Immunol.*, 2010, **47**, 1421–1425.
51 J. Gorga, A. Dong, M. Manning, R. Woody, W. Caughey and J. Strominger, *Proc. Natl. Acad. Sci. U. S. A.*, 1989, **86**, 2321–2325.
52 A. M. Abdul-Fattah, V. Truong-Le, L. Yee, L. Nguyen, D. S. Kalonia, M. T. Cicerone and M. J. Pikal, *J. Pharm. Sci.*, 2007, **96**, 1983–2008.
53 B. Shivu, S. Seshadri, J. Li, K. A. Oberg, V. N. Uversky and A. L. Fink, *Biochemistry*, 2013, **52**, 5176–5183.
54 Aniket, D. A. Gaul, D. L. Rickard and D. Needham, *J. Pharm. Sci.*, 2014, **103**, 810–820.
55 U. Andreasson, A. Perret-Liaudet, L. van Waalwijk van Doorn, K. Blennow, D. Chiasserini, S. Engelborghs, T. Fladby, S. Genc, N. Kruse, H. B. Kuiperij, L. Kulic, P. Lewczuk, B. Mollenhauer, B. Mroczko, L. Parnetti, E. Vanmechelen, M. M. Verbeek, B. Winblad, H. Zetterberg, M. Koel-Simmelink and C. E. Teunissen, *Front. Neurol.*, 2015, **6**, 179.
56 M. Ovacik and K. Lin, *Clin. Transl. Sci.*, 2018, **11**, 540–552.